The Pros and Cons of Wall Functions

Conference Paper · July 2015

DOI: 10.1115/OMAE2015-41518

CITATIONS
2

READS
652

4 authors:

Luís Eça
Technical University of Lisbon
91 PUBLICATIONS **836** CITATIONS
SEE PROFILE

Guilherme Vaz
Maritime Research Institute Netherlands
118 PUBLICATIONS **764** CITATIONS
SEE PROFILE

Hugo Abreu
Technical University of Lisbon
7 PUBLICATIONS **3** CITATIONS
SEE PROFILE

Gonçalo Saraiva
Technical University of Lisbon
1 PUBLICATION **2** CITATIONS
SEE PROFILE

Proceedings of ASME 34rd International Conference on Ocean, Offshore and Arctic Engineering
OMAE2015
June 1-6, 2015, St John's, NL, Canada

OMAE2015-41518

THE PROS AND CONS OF WALL FUNCTIONS

Luís Eça
IST-UL
Mechanical Engineering Department
Av. Rovisco Pais 1, 1049-001 Lisboa
Portugal
Email: luis.eca@ist.utl.pt

Gonçalo Saraiva
IST-UL
Mechanical Engineering Department
Av. Rovisco Pais 1, 1049-001 Lisboa
Portugal
Email: gsaraiva8@gmail.com

Guilherme Vaz
MARIN
R&D Department, CFD Projects
P.O. Box 28, 6700 AA Wageningen
The Netherlands
Email: g.vaz@marin.nl

Hugo Abreu
IST-UL
Mechanical Engineering Department
Av. Rovisco Pais 1, 1049-001 Lisboa
Portugal
Email: hugo.abreu.91@gmail.com

ABSTRACT

Simulations of viscous flows based on the Reynolds-Averaged Navier-Stokes (RANS) equations have become an engineering tool used on a daily basis. One of the main goals of such calculations is to determine friction forces, which are a consequence of the shear-stress at solid walls.

In RANS (and other more sophisticated mathematical models), there are two main approaches for the determination of the shear-stress at a wall: direct application of the no-slip condition, i.e. the velocity gradient is determined directly at the surface; wall functions which determine the shear-stress at the wall from semi-empirical equations applicable up to the outer edge of the so-called "wall layer/log layer". Although the first option is physically preferable, its numerical requirements may lead to iterative convergence problems and/or excessive calculation times. Therefore, especially at high Reynolds numbers, it is not unusual to use the latter approach.

In this paper we discuss the advantages and disadvantages of wall-function boundary conditions. To this end we have calculated the flow around a flat plate, conventional and laminar airfoils and a circular cylinder. The influence of the location where wall functions are applied (distance to the wall) and the effect of the Reynolds number (ranging from model to full scale applications) are discussed. Griding requirements for wall-function boundary conditions are also addressed. The results obtained with wall functions are compared with those obtained from the direct application of the no slip at the wall.

The results obtained in this study show that the use of wall functions in viscous flow calculations may be justifiable or completely unacceptable depending on the flow conditions. Furthermore, it is also shown that wall-function boundary conditions also require clustering of grid nodes close to the wall, but obviously less demanding than the direct application of no slip condition.

INTRODUCTION

Simulations of viscous flows based on the Reynolds-Averaged Navier-Stokes (RANS) equations have become an engineering tool used on a daily basis. One of the main goals of such calculations is to determine friction forces, which are a consequence of the shear-stress at solid walls.

Near-wall flow fields at high Reynolds numbers (typical of Naval and Offshore applications) exhibit large gradients and so the accurate determination of friction forces is still a modelling and numerical challenge. The boundary conditions of the RANS equations at solid (and impermeable) walls impose the velocity components. In RANS (and other more sophisticated mathematical models), there are two main approaches for the determination of the shear-stress at a wall: direct application of the no-slip condition, i.e. the velocity gradient is determined directly at the surface; wall functions which determine the shear-stress at the wall from semi-empirical equations applicable up to the outer edge of the so-called "wall-layer/log-layer".

The main (and only) drawback of the first approach is the extremely small vertical size of the near-wall cells (typically 1 dimensionless wall unit $y^+ \simeq 1$) that leads to higher cell counts and cells with high aspect ratio that make iterative convergence troublesome or even impossible. On the other hand, the main

advantage of wall-function boundary conditions is the ability to increase significantly (it can reach $y^+ \simeq 10^3$ in full scale calculations) the size of the near-wall cells, reducing the number of cells and making iterative convergence easiest to achieve. Nonetheless, there are two facts that must be recognized in the use of wall functions:

1. Wall-function boundary conditions are part of the mathematical model adopted to solve viscous flows, i.e. of the problem definition (computational domain, set of equations and boundary conditions).
2. The motivation for their use is to facilitate the numerical solution of the problem[1] at the cost of the accuracy of the modelling.

This latter aspect implied that the use of wall functions started to be questioned 30 years ago [1]. However, the appearance of the so-called "automatic" wall functions, see for example [2,3], that blended the linear sub-layer with the log-layer gave a new increase to the use of wall functions [5, 6, 7, 8, 9]. These days there is a widespread use of wall-function boundary conditions in highly complex ship geometries [10] and/or with turbulence closures more sophisticated than simple eddy-viscosity models for RANS solvers [11, 12]. In offshore applications, it is also common practice to adopt wall functions, as the papers submitted to the OMAE Conferences on Ocean, Offshore and Arctic Engineering of recent years demonstrate, as for example [13].

It is undeniable that "automatic" wall functions have improved significantly the numerical robustness of its application by comparing with the standard wall functions based only on the "log-law" region. The main advantage of the approach is that it is (almost) equivalent to the direct application of the no slip condition when the near-wall cell has $y^+ < 1$. However, in that case, wall functions are not needed. On the other hand, the physical limitations of the approach remain present:

- The log-law is derived for a statistically steady, two-dimensional, zero pressure gradient flow that leads to a constant total shear-stress in the near-wall region, i.e. the sum of the mean and Reynolds shear-stresses matches the shear-stress at the wall τ_w. In other circumstances (i.e. for almost any flow) it is at best a crude approximation of the real flow.
- The proposed solutions for the buffer-layer [2, 3] are simple algebraic blends that do not have any physical support.

Therefore, it is mandatory to assess the consequences of the approach in the predicted flow field. To this end we have selected four test cases to check the consequences of the use of wall-function boundary conditions when compared with solutions obtained with the direct application of the no-slip condition:

- Flow over a flat plate with Reynolds numbers ranging from 10^7 to 10^9.
- Flow around the NACA 0012 airfoil at 0^o and 4^o degrees angle of attack and Reynolds number equal to 6×10^6.
- Flow around a Eppler 374 airfol at 0^o degrees angle of attack and Reynolds number equal to 3×10^5.
- Flow around a circular cylinder at Reynolds numbers of 6.31×10^4 and 2.52×10^5.

[1]Even in the case of flows over rough surfaces, the use of wall-function boundary conditions is mainly motivated by "numerical reasons" [4].

It can be argued that we have selected only two-dimensional test cases. However, the performance of wall-function modelling may be expected to be worse in three-dimensional flow than in two-dimensional flow; the flow over a flat plate is the best case scenario for the evaluation of wall functions. Furthermore, it has been shown that the predicted friction resistance of a simple flat plate flow obtained with the two-equation shear-stress transport (SST) $k-\omega$ [15] is dependent on the location where the wall-function boundary conditions are applied [4]. Also, in the present study we want to investigate the effect of selecting near-wall grid cells that exhibit increasing height, which is common practice for most "wall-function grids" generated by commercial grid generators.

The investigation reported in this paper was performed with the ReFRESCO [14] flow solver using the two-equation shear-stress transport (SST) $k-\omega$ [15] turbulence model. All flow fields were calculated with a sufficient number of geometrically similar grids (and time steps) to assess the numerical uncertainty. This will allow us to judge if the present results have more than just qualitative value.

Section 2 presents the wall functions formulation tested in this study and the main features of the flow solver ReFRESCO are briefly described in section 3; the results are presented and discussed in section 4 and the conclusions are summarized in section 5.

WALL BOUNDARY CONDITIONS

At a solid wall the three components of the mean velocity are equal to the wall velocity. The no-slip condition imposes the two components tangential to the wall and the impermeability condition specifies the component normal to the wall. At high Reynolds number, the standard condition for the mean pressure is zero derivative in the normal direction to the wall.

The turbulence kinetic energy at the wall is zero $k = 0$, but ω goes to infinity. However, there is a near-wall analytic solution for the ω transport equation [16]

$$\omega = \frac{6}{\beta\,(y)^2}\,, \tag{1}$$

where $\beta = 0.075$ and y is the distance to the wall. This allows the specification of ω at the centre of near-wall cell [17] when the grid cell size corresponds to $y^+ < 1$, where

$$y^+ = \frac{u_\tau y}{\nu} \text{ and } u_\tau = \sqrt{\frac{\tau_w}{\rho}}\,.$$

τ_w is the shear-stress at the wall and ν and ρ are the kinematic viscosity and density of the fluid, respectively.

When the near-wall cell size is sufficiently small ($y^+ < 1$), the shear-stress at the wall is determined directly from its definition

$$\tau_w = \mu \frac{\partial U_t}{\partial y} \simeq \mu \frac{(U_t)_c}{y_c}\,, \tag{2}$$

where $\mu = \rho\nu$, U_t is the velocity parallel to the wall and the subscript $_c$ designates values at the near-wall cell centre. The restrictions imposed to the near-wall cell size to apply equation (2) may

lead to iterative convergence difficulties at high Reynolds numbers. This is an incentive to increase the size of the near-wall cell and adopt wall-function boundary conditions (designated by WF in the remaining of the paper). However, this motivation for the use of WF is purely numerical.

Another issue discussed below, is that the use of WF should still imply that the near-wall grid has enough resolution to capture the high gradients of the boundary-layer. However, this is not common practice in commercial grid generators, where grids for WF application have cell sizes that increase with the distance to the wall. Such practice leads to grids that are too coarse in the region above the near-wall cell (see Figure 1).

With wall functions, the boundary conditions for the mean flow quantities remain exactly the same. On the other hand, the determination of τ_w and of the turbulence quantities require modifications as explained below.

Determination of wall shear-stress

The blend of the linear sub-layer with the log-layer proposed in [2] is

$$u^+ = \frac{U}{\tau_w} = \left(\left(\frac{1}{y^+} \right)^4 + \left(\frac{\kappa}{\ln(y^+ E)} \right)^4 \right)^{-0.25} \qquad (3)$$

with $\kappa = 0.41$ and $E = 8.43$. Equation (3) is solved at the centre of the near-wall cells to determine τ_w.

With this approach y_c may be located up to the outer edge of the log-layer (wherever it is located). Nonetheless, the main advantage of equation (3) is that it becomes equivalent to equation (2) when $y_c^+ < 1$.

There are two points that should be mentioned for the determination of τ_w:

1. Equation (3) is not the only proposal available in the open literature to blend the linear and log layers. Nonetheless, the results presented in [18] for ship flows with two different alternatives are qualitatively similar.
2. There are other alternatives proposed in the open literature (see for example [7]) that combine the result obtained from equation (3) with the determination of the turbulence kinetic energy k at the near-wall cell. Three alternatives were tested[2] in [4] and the best results were obtained with the present choice.

Turbulence quantities

With WF, ω is also specified at the centre of the near-wall cells using the blend proposed in [2]

$$\omega^+ = \left(\left(\frac{6}{\beta\,(y^+)^2} \right)^2 + \left(\frac{1}{\kappa\sqrt{C_\mu}\,y^+} \right)^2 \right)^{0.5}, \qquad (4)$$

where $C_\mu = 0.09$.

There are several alternatives for the turbulence kinetic energy boundary condition:

1. Impose $k = 0$ at the wall and solve the k transport equation with the production term in the near-wall cell determined from the shear-stress at the wall and the derivative of u^+ with respect to y^+, which is obtained from equation (3).
2. Impose k at the near-wall cells centre with a blend of the linear and log sub-layers.
3. Apply zero normal derivative to k, which is the approach followed by standard wall functions [7].

In [19], it has been demonstrated that the latter approach is not a good choice for the k boundary condition with "automatic" wall functions. Although we tested the other two options, we will restrict ourselves to the results obtained with the first alternative. Nonetheless, it must be mentioned that correcting the production term of the k equation in the near-wall cell makes WF slightly different from NS even when the near-wall cell is inside the linear sub-layer.

FLOW SOLVER

ReFRESCO [20] is a CFD code that solves multi-phase (unsteady) incompressible flows with the RANS equations, complemented with turbulence models, cavitation models and volume-fraction transport equations for different phases [14]. Discretization is based on a finite-volume approach with cell-centered collocated variables. The equations are discretized in strong-conservation form and a pressure-correction equation based on the SIMPLE algorithm (see for example Ferziger & Péric [21]) is used to ensure mass conservation. Time integration is performed implicitly with first or second-order backward schemes. At each implicit time step, the non-linear system for velocity and pressure is linearized with Picard's method and the coupled linear system is solved with a matrix-free Krylov subspace method using a SIMPLE-type preconditioner [22]. A segregated approach is adopted for the solution of the turbulence model equations.

The implementation is face-based, which permits grids with elements consisting of an arbitrary number of faces (hexahedrals, tetrahedrals, prisms, pyramids, etc.), and if needed h-refinement (hanging nodes). The code is parallelized using MPI and sub-domain decomposition, and runs on Linux workstations, clusters and super-computers. ReFRESCO (v2.1.0) is currently being developed, verified and validated at MARIN (in the Netherlands) [14] in collaboration with IST (in Portugal) [23], USP-TPN (University of São Paulo, Brasil) [24], TUDelft (Technical University of Delft, the Netherlands) [22], UoS (University of Southampton, UK) [26], and recently UTwente (University of Twente, the Netherlands) and Chalmers (Chalmers University, Sweden).

RESULTS

We have selected four two-dimensional test cases of different complexity to assess the consequences of the use of WF. Our aim is to check the influence of size of the near-wall cell in the flow solution. Furthermore, we will also assess the gridding requirements for the use of WF.

All the calculations presented below were performed with double precision and so round-off errors are negligible when

[2] Boundary conditions for rough walls are discussed in the same reference and so they will not be discussed in this paper.

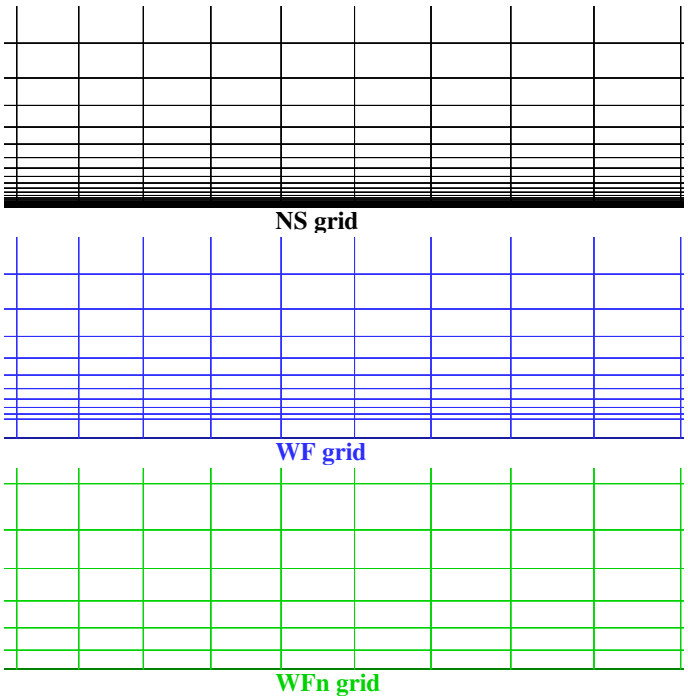

Figure 1. Illustration of the grids for the calculation of the flow over a flat plate in the near-wall region.

compared to the discretization errors. Convergence criteria of iterative errors imposes a reduction of the L_∞ norm of the normalized residuals[3] of all transport equations to values below 10^{-7}. Therefore, numerical errors are dominated by the discretization error, which are assessed using the procedure proposed in [27] with at least four grids that cover a grid refinement ratio of 2.

Flat plate

The first test case is the flow over a flat plate at Reynolds numbers $Rn = U_\infty L/\nu$ based on the undisturbed velocity U_∞ and plate length L of 10^7, 10^8 and 10^9. The computational domain is a rectangle with a length of $1.5L$ and a width of $0.25L$ ($-0.25L < x < 1.25L$ and $0 < y < 0.25L$). The inlet boundary is located $0.25L$ upstream of the leading edge of the plate and the outlet boundary $0.25L$ downstream of the trailing edge. It has been checked in [4, 19, 28] that with these options the results are not affected by the limited domain size.

Undisturbed velocity is imposed at the inlet and the pressure is imposed at the top boundary. Normal derivatives of remaining dependent variables are set equal to zero at the top boundary and streamwise derivatives of all dependent variables are set equal to zero at the outlet. At the bottom boundary, symmetry conditions are applied upstream and downstream of the plate ($-0.25L < x < 0$ and $L < x < 1.25L$). k and ω are specified at the inlet from the following conditions: turbulence intensity is equal to 1% and $(\nu_t/\nu)(1/Rn) = 10^{-9}$.

We have generated three types of orthogonal stretched grids for the present calculations:

- Grids with the near-wall cell size appropriate for the direct application of the no slip condition, NS grids. The finest grids have 1537 nodes in the horizontal direction and 193 ($Rn = 10^7$), 257 ($Rn = 10^8$) and 321 ($Rn = 10^9$) in the vertical direction.
- WF grids that are obtained from the previous ones removing cells close to the wall to increase the size of the near-wall cell. The number of cells removed in each grids set is proportional to the refinement level to guarantee that the size of the near-wall cells remains the same, which is crucial for a proper uncertainty analysis.
- WFn grids that have the same near-wall cell of the WF grids but a cell size that increases with the distance to the wall, which is the typical distribution of cell sizes generated by commercial grid generators for the application of WF.

In the first two cases it is straightforward to generate sets of geometrically similar grids, whereas for the latter case it is not possible to keep the near-wall cell size fixed and preserve geometrical similarity. Therefore, the calculations in the WFn

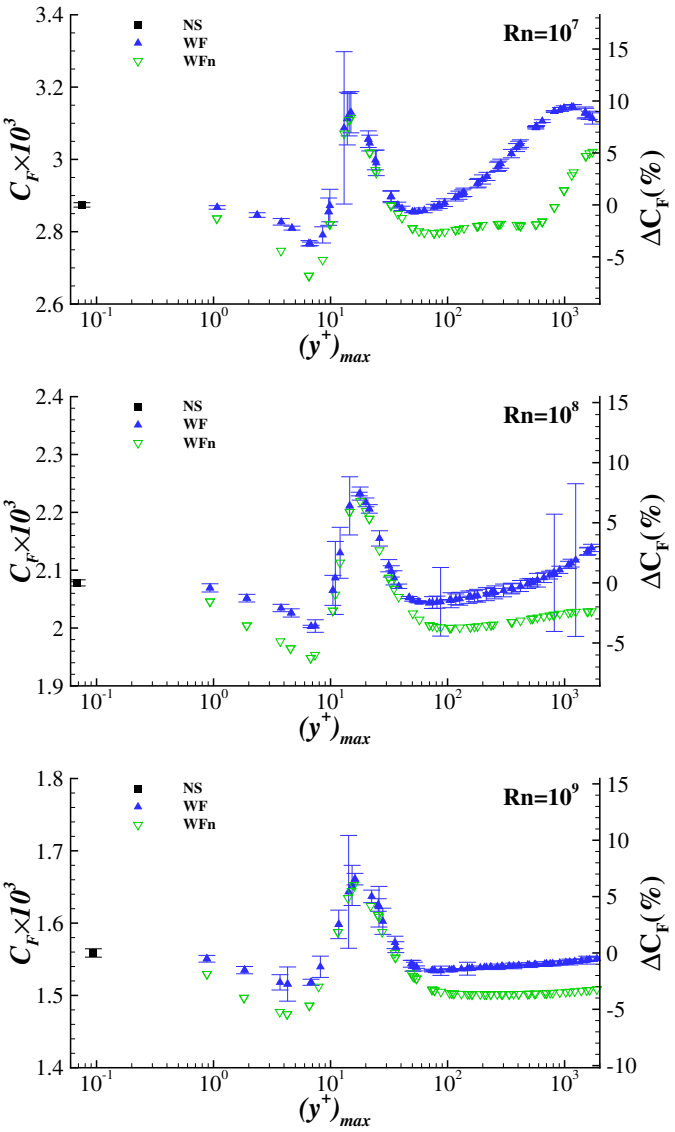

Figure 2. Friction resistance coefficient C_F of a flat plate as a function of $(y^+)_{max}$ of the near-wall cells. Right vertical axis indicates differences to NS solution.

[3]The residuals are normalized by the main diagonal of the system and so its value corresponds to the variable change in a simple Jacobi iteration.

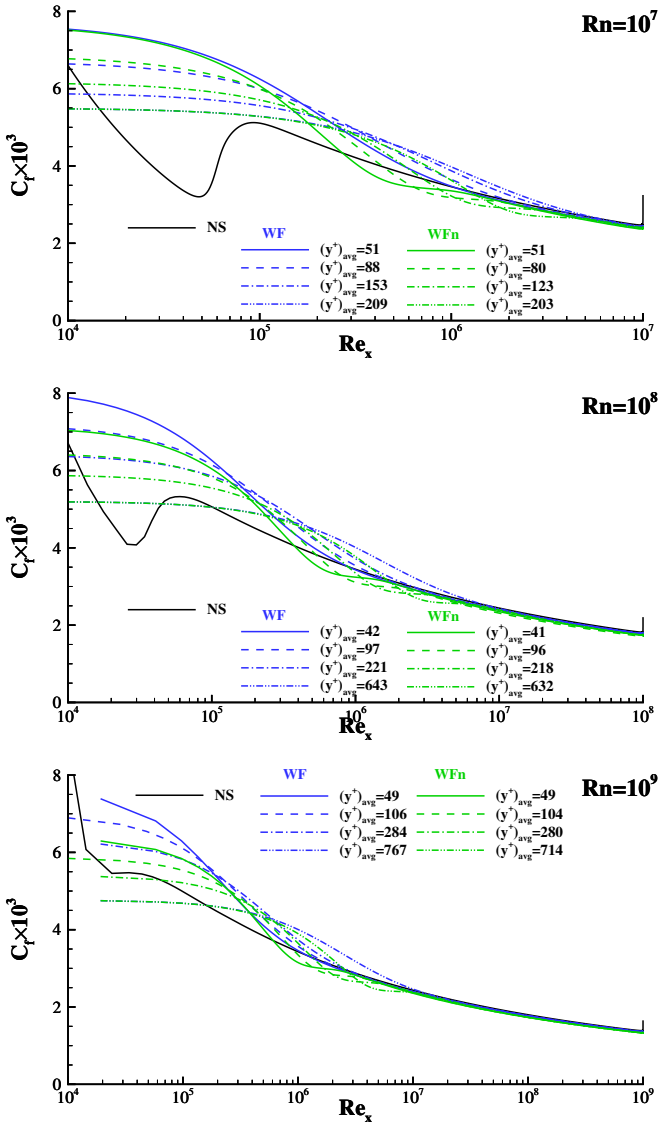

Figure 3. Skin friction coefficient C_f along the plate ($Re_x = Rn(x/L)$) for different sizes of the near-wall cells identified by the average y^+_{avg}.

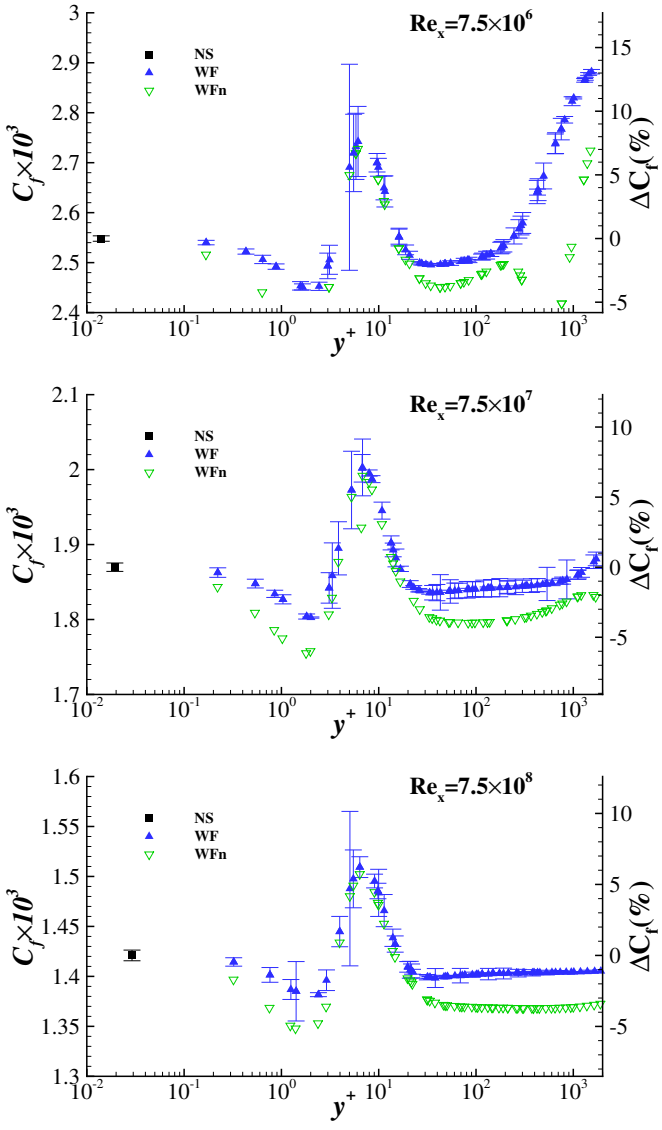

Figure 4. Skin friction coefficient C_f at $(x/L = 0.75)$ as a function of the size of the near-wall cells identified by y^+. Right vertical axis indicates differences to NS solution.

sets were performed only for the level of refinement of the finest grids of the WF sets.

Figure 1 illustrates the three types of grids in the near-wall region. In the WF grids the smallest vertical size of the cells is above the near-wall cell, whereas in the WFn grids near-wall cells exhibit the smallest vertical cell size. It is clear that the level of grid refinement of the WFn grids in the boundary-layer region may become insufficient with the increase of the size of the near-wall cells.

The finest grids of the NS sets used to produce the reference solution with the direct application of the no slip condition have values of the maximum y^+ of the near-wall cells close to 0.08 for the three Reynolds numbers. To check the application of WF, we have generated 64 sets of grids with a near-wall cell size that covers a range of y^+ values that includes the linear, buffer and log layers. For each of these 64 cases, we have also made 64 WFn grids with the same refinement level.

Figure 2 presents the predicted friction resistance coefficient C_f[4] of the plate as a function of the $(y^+)_{max}$ of the near-wall cells. The results exhibit several interesting features:

- There is a significant influence of the size of the near-wall cells in the predicted C_F with WF for the three Reynolds numbers tested. For values of y^+ in the buffer-layer the deviations to the NS solution reach values close to 10%.
- The range of cell sizes that lead to an approximately constant C_F is strongly affected by the Reynolds number. However, even at $Rn = 10^9$ (that exhibits the largest range) there is a difference of approximately 1% between the WF and NS solutions which is larger than the numerical uncertainty.
- Curiously, the WFn grids show a wider region of y^+ with C_F approximately constant than the WF grids. However, the deviation to the NS solution is close to 3% for the three Reynolds numbers tested.
- For the WF grids, the numerical uncertainties are in general

[4] $C_f = \tau_w / (1/2\rho U_\infty^2)$.

the highest in the buffer layer, for all three Reynolds numbers.

The results presented in figure 2 are a consequence of the integration of the skin friction coefficient along the plate, which is depicted in figure 3 for the NS solution and 4 different WF and WFn solutions. As expected [4, 28], the NS solution exhibits a "transition" region located between $Re_x = 5\times10^4$ and $Re_x = 10^5$, which is one order of magnitude smaller than what is observed in experiments [29]. Nonetheless, upstream of the "transition region" the NS solution matches the Blasius solution.

On the other hand, none of the WF solutions exhibits a laminar flow region and the shear-stress at the wall for $Re_x < 10^6$ is strongly dependent on the size of the near-wall cells for all Reynolds numbers. Naturally, the largest impact of such result on C_F is observed at $Rn = 10^7$ where 50% of the plate exhibits a significant difference between the NS and WF solutions.

The WF solutions approach the NS predictions for $Re_x > 5\times10^6$, but the WFn results exhibit a nonphysical oscillation at $Re_x \simeq 10^6$ and a level of C_f for $Re_x > 5\times10^6$ below the NS prediction. This means that the smaller dependency of C_F on $(y^+)_{max}$ in the WFn grids is a consequence of error cancelling.

The trends discussed above are confirmed by the skin friction coefficient (C_f) predictions at $(x/L = 0.75)$, which are presented in figure 4. The difference between the NS and WF solutions for y^+ in the log-layer is close to 1%, whereas a 3% difference is obtained for the WFn grids. The inaccuracy of the "automatic" wall functions approach for values of y^+ in the buffer-layer is evident.

Airfoils

The following test cases are the flows around two airfoils: the NACA 0012 at 0^o and 4^o degrees angle of attack for a Reynolds number of 6×10^6; the Eppler 374 at 0^o degrees angle of attack and $Rn = 3\times10^5$. The first is a classical test case for which there are many experimental and numerical results available [30], whereas the second is a laminar airfoil at a low Reynolds number[5].

The calculation domain is a rectangle of 36 chords length (inlet 12 chords upstream of the leading edge) and 24 chords width. Velocity components and turbulence quantities are specified at the inlet and all streamwise derivatives are assumed to be zero at the outlet. At the top and bottom boundaries, normal derivatives are set equal to zero and the pressure is imposed at the top left corner of the domain.

As for the flat plate, we have generated sets of geometrically similar grids for the direct application of the no slip condition (NS) and two types of grids for wall-function boundary conditions: grid sets obtained from the NS grid removing lines close to the wall (WF); grids with an increasing vertical spacing in the near-wall region (WFn). The finest grids of the NS sets include 929280 cells and the coarsest 232320. The computational domain and the grid sets are illustrated in figure 5 for a grid with only 14520 cells, which is much coarser than all the grids used.

[5]Naturally, we are aware that these are flow conditions where WF became undoubtedly questionable. However, we purposely intend to illustrate the effects of using WF in these conditions.

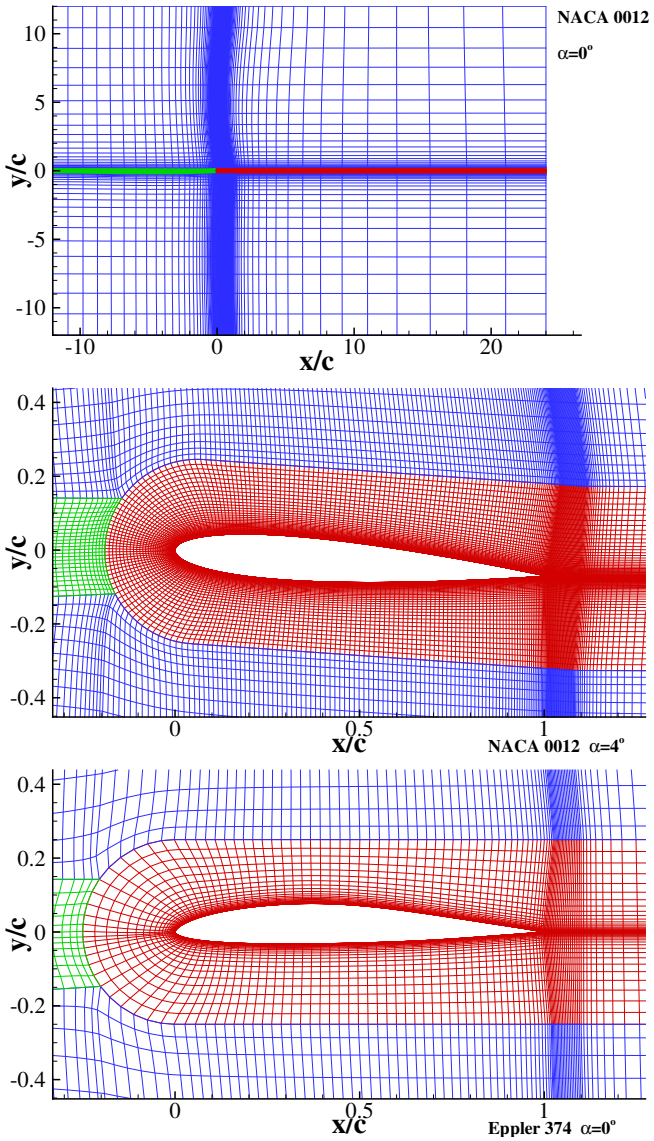

Figure 5. Computational domain and typical multi-block grids for the calculation of the flow around the NACA 0012 and Eppler 374 airfoils.

The quantities of interest for the flow around the airfoils are the friction Cd_f and pressure Cd_p drag coefficients, the lift coefficient Cl and the surface distributions of pressure C_p and skin friction C_f coefficients.

NACA 0012 airfoil

The results obtained for the Cd_f and Cd_p drag coefficients at 0^o degrees angle of attack are presented in figure 6. The trends observed in Cd_f are similar to those obtained for the flat plate flow. On the other hand, Cd_p shows less sensitivity to the size of the near wall cells but the small peak in the buffer-layer region is also visible.

The Cd_f and Cd_p drag coefficients are a consequence of the C_p and C_f coefficients[6] distributions on the airfoil surface, which are depicted in figure 7. The results obtained without wall functions are in excellent agreement with the reference solution given in [30]. However, the C_f prediction with wall-function boundary

[6]$C_p = (p - p_\infty) / (1/2\rho U_\infty^2)$.

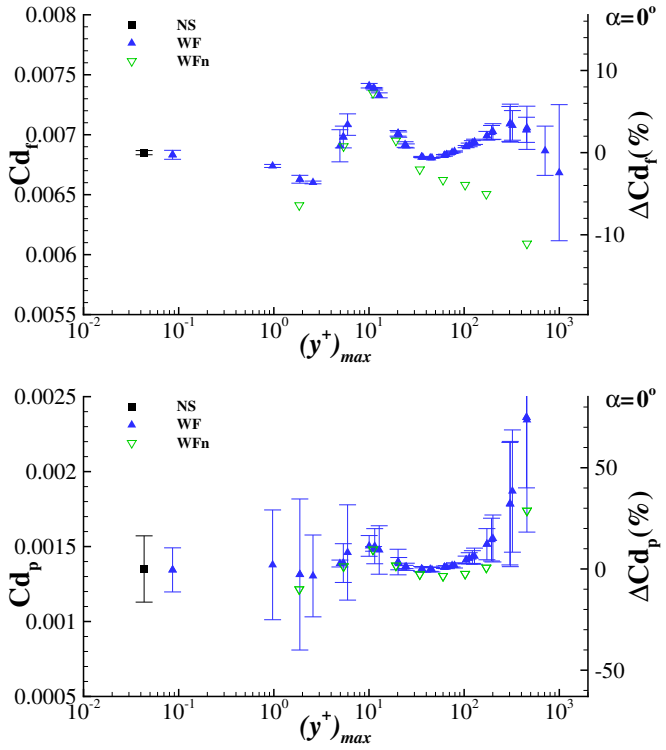

Figure 6. Friction Cd_f and pressure Cd_p drag coefficients of the NACA 0012 at $\alpha = 0^o$ and $Rn = 6 \times 10^6$. Right vertical axis indicates differences to NS solution.

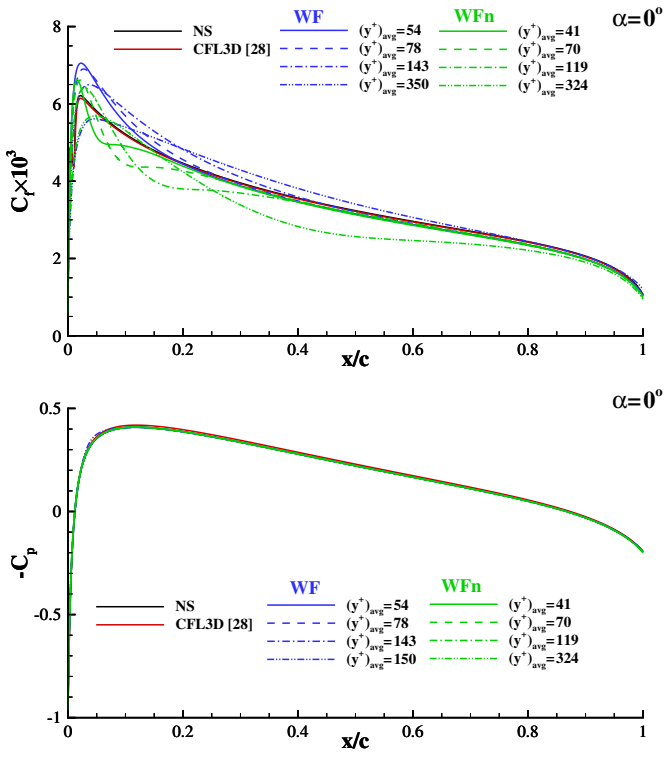

Figure 7. Friction Cd_f and pressure Cd_p drag coefficients of the NACA 0012 at $\alpha = 0^o$ and $Rn = 6 \times 10^6$.

conditions is significantly different and strongly affected by the near-wall cell size. The results obtained with the WFn grids exhibit again nonphysical oscillations. The graphical agreement of

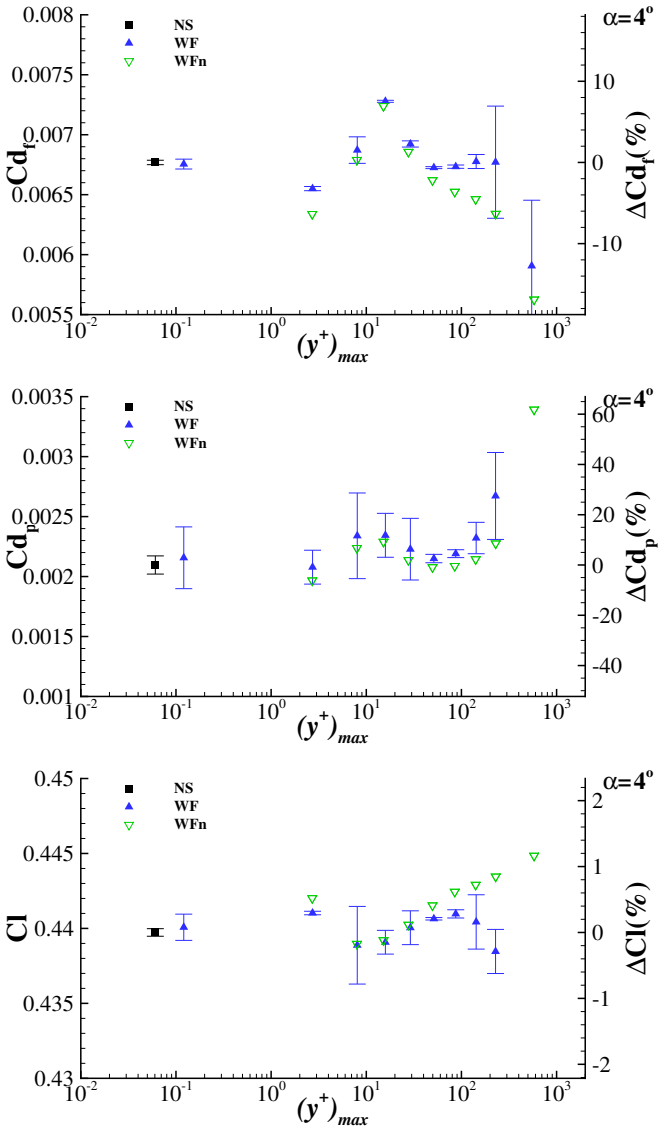

Figure 8. Friction Cd_f and pressure Cd_p drag coefficients and lift C_l coefficient of the NACA 0012 at $\alpha = 4^o$ and $Rn = 6 \times 10^6$. Right vertical axis indicates differences to NS solution.

the several pressure distributions seems reasonable. However, for $y^+_{avg} = 324$, the difference between the NS and WFn predictions is close to 30%. This is an excellent example of how simple graphical comparisons may lead to misleading conclusions, because 30% difference is seldom classified as reasonable.

Figure 8 presents the Cd_f, Cd_p and C_l for $\alpha = 4^o$. The results obtained for the drag coefficients exhibit similar trends to those obtained at $\alpha = 0^o$. On the other hand, the lift coefficient shows a significant smaller influence of the nearest wall cell size with wall-function boundary conditions. Nonetheless, the WFn grids lead to larger differences to the NS solution than the WF grids, but still below 1%.

The C_f and C_p distributions for $\alpha = 4^o$ are presented in figure 9. The region with the largest discrepancies between the NS and WF and WFn solutions is the first 25% of the chord with the poorest results obtained for the WFn grids. Once again, the agreement between the different C_p distributions is much better than for C_f.

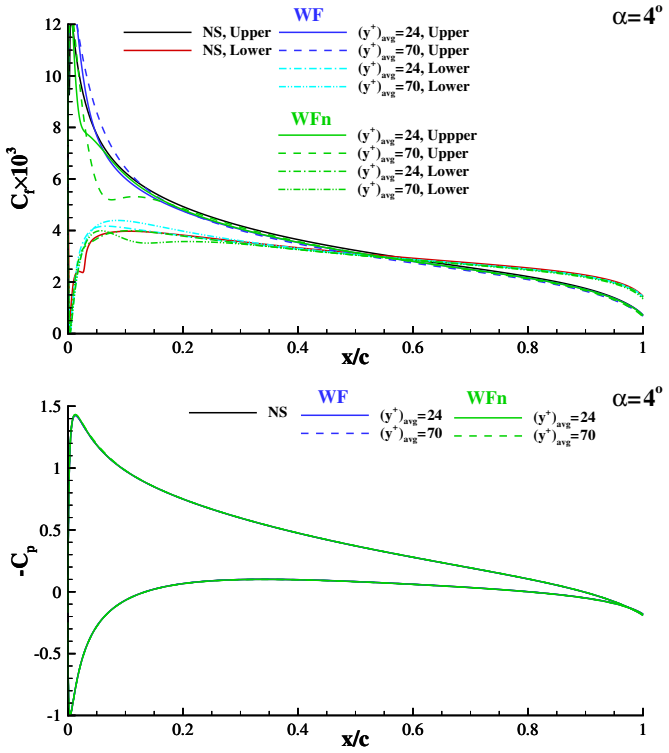

Figure 9. Friction Cd_f and pressure Cd_p drag coefficients of the NACA 0012 at $\alpha = 4^o$ and $Rn = 6 \times 10^6$.

Eppler 374 airfoil

Figure 10 presents Cd_f, Cd_p and Cl obtained for the different grid sets tested. The first remark that must be made is that the range of sizes of the near-wall cells for the application of wall-function boundary conditions is much smaller than in the previous test cases. This is a consequence of the selected Reynolds number.

As expected, this test case exhibits much larger differences between the NS and WF and WFn solutions than the previous ones. The discrepancies are also visible in Cl that changes almost for all the range of near-wall cell size tested. It should be mentioned that the iterative convergence properties of the WF and WFn solutions are significantly worse than those obtained with NS.

These poor results obtained for the WF and WFn grids are explained by the C_f and C_p distributions depicted in figure 11. Although the NS solution exhibits transition upstream of the adverse pressure gradient region of the upper surface, there is clearly a laminar flow region for the upper and lower surface boundary-layers. On the other other hand, wall-function boundary conditions eliminate the laminar flow region and the WF and WFn solutions do not show any resemblance to the NS results. Furthermore, for $(y^+)_{avg} = 70$, there is also poor agreement for the C_p distribution. Therefore, wall-function boundary conditions are clearly inadequate for this type of applications.

Circular cylinder

The last test case is the classical statistically periodic unsteady flow around a smooth circular cylinder. We have selected

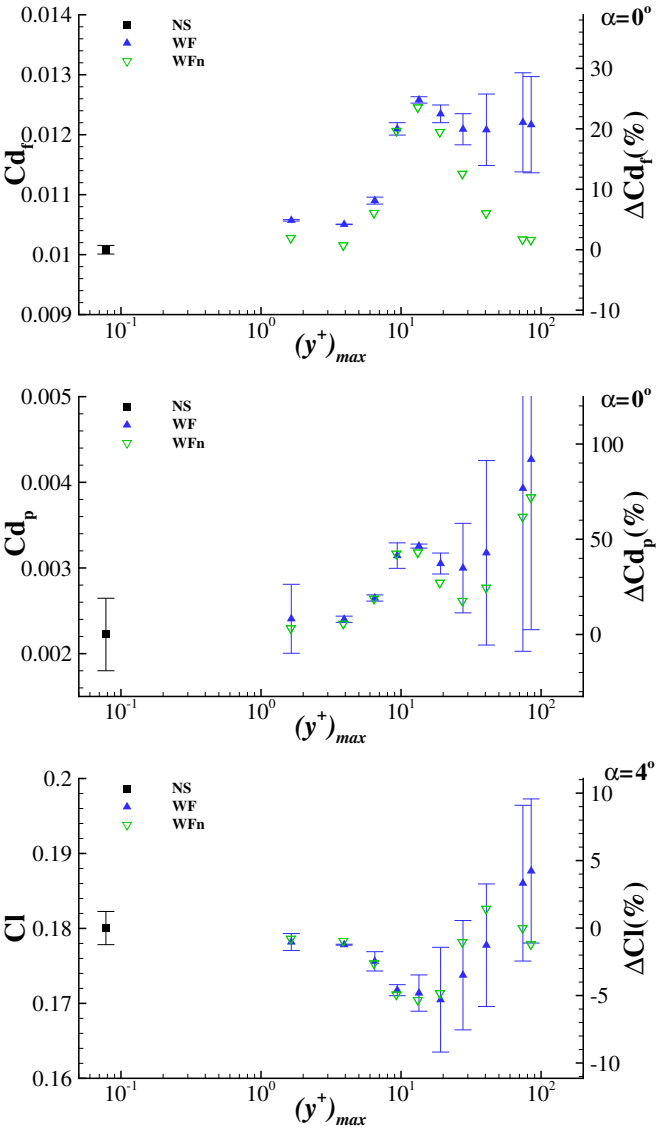

Figure 10. Friction Cd_f and pressure Cd_p drag coefficients and lift C_l coefficient of the Eppler at $\alpha = 0^o$ and $Rn = 3 \times 10^5$.

two Reynolds numbers[7]: $Rn = 6.31 \times 10^4$ that is clearly below drag crisis[8] and $Rn = 2.52 \times 10^5$ which is just at the beginning of drag crisis[9].

The computational domain follows the suggestions of [31] and the boundary conditions are equivalent to those applied in the calculation of the flow around the airfoils. In this case, we have only tested one NS and WF grid set[10] (for each Rn). $(y^+)_{max}$ of the WF grids is close to 45. The grids have at least 960 cells on the cylinder surface and a grid with one quarter of the cells used in the coarsest grid of each set is illustrated in figure 12. The refinement in space is consistent with the time refinement and the average Courant number is close to 4. The results presented below were obtained from the average of the last 8 cycles

[7] For this flow $Rn = U_\infty D/\nu$ where D is the diameter of the cylinder.

[8] Once more, we are aware that the flow upstream of the separation points should be laminar.

[9] This will be demonstrated by the three experimental values of the average drag coefficient Cd_{avg} included in figure 13.

[10] For $Rn = 6.31 \times 10^4$ we have calculated only one single grid with WF due to the poor quality of the results.

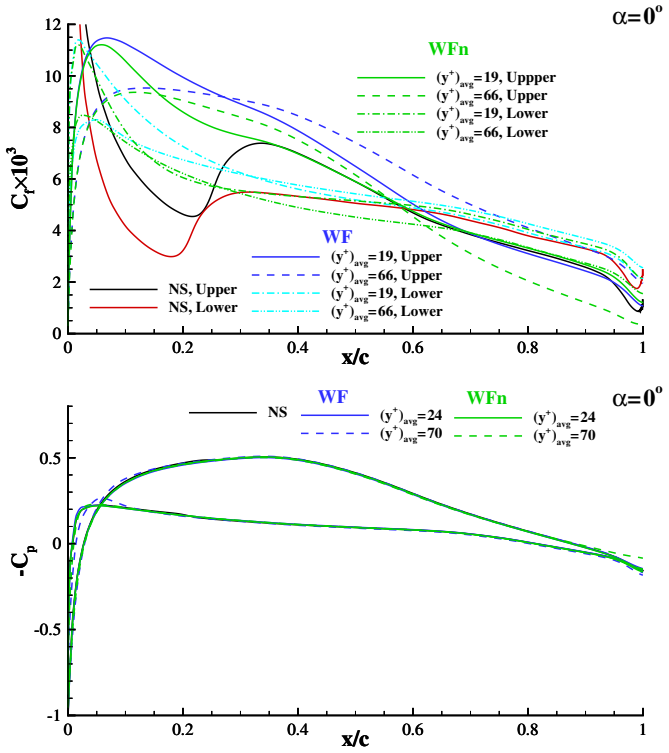

Figure 11. Friction Cd_f and pressure Cd_p drag coefficients of the Eppler 374 at $\alpha = 0^o$ and $Rn = 3 \times 10^5$.

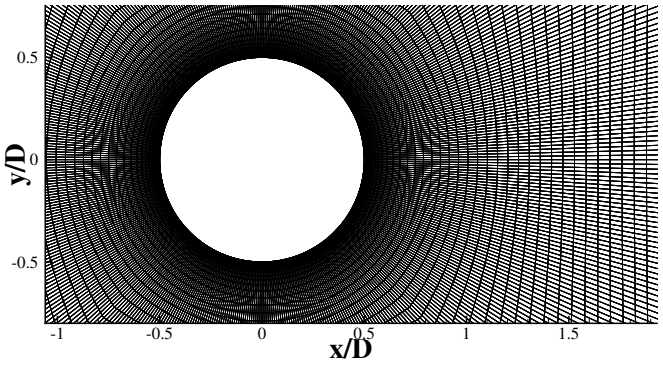

Figure 12. Illustration of the grids for the calculation of the flow around a circular cylinder.

computed.

Figure 13 presents the average drag coefficient obtained for the two Reynolds numbers with NS and WF as a function of the refinement ratio (λ_i/λ_1). The plot includes the best fit to the data and the experimental results obtained from the review presented in [32]. Although it is well known that the SST model will not be able to match the experimental results for these Reynolds numbers [24], with NS we capture the correct trend with the Reynolds number. The result obtained with WF at $Rn = 6.31 \times 10^4$ is completely wrong ($Cd_{avg} = 0.33$) and for $Rn = 2.52 \times 10^5$ the differences to the solution obtained with NS are clearly larger than the numerical uncertainty.

The results obtained for Cd_{avg} are justified by the mean C_p and C_f distributions on the cylinder surface that are presented in figure 14. WF lead to the smallest separation regions in the wake, especially at $Rn = 6.31 \times 10^4$ where the mean separation angle

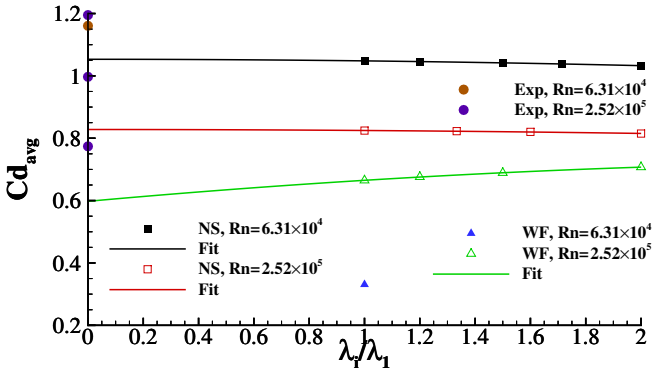

Figure 13. Average drag coefficient Cd_{avg} of the flow around a circular cylinder as a function of the refinement ratio $\lambda_i/lambda_1$. Experimental values of different source are plotted for $\lambda_i/lambda_1 = 0$.

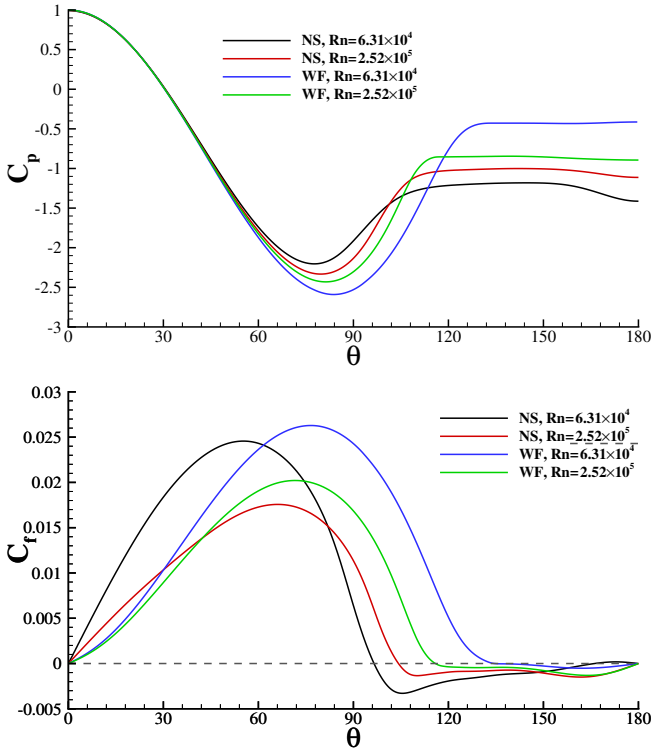

Figure 14. Mean pressure C_p and skin friction C_f coefficients on the cylinder surface. $\theta = 0^o$ on the side of the cylinder facing the incoming flow.

is close to 130^o. As a consequence, the base pressure coefficient ($\theta = 180^o$) is too large in the WF predictions. This poor performance of WF is not unexpected because the flow is supposed to remain laminar up to the separation point and WF make the flow "fully-turbulent".

It should also be mentioned that as for the Eppler airfoil the iterative convergence properties of the WF calculations at these Reynolds number are worse than those obtained with the direct application of the no-slip condition.

CONCLUSIONS

This paper presents an assessment of the consequences of

the use of wall functions in the calculation of viscous flows with the RANS equations supplemented with the SST two-equation $k-\omega$ eddy-viscosity turbulence model.

Calculations were performed with and without wall functions for the following test cases: a flat plate, the NACA 0012 and Eppler 374 airfoils and a circular cylinder. The Reynolds number ranges from values that correspond to significant parts of laminar flow (flat plate, Eppler 374 and circular cylinder) to values that lead to flows with negligible parts of laminar flow (flat plate and NACA 0012).

The influence of the near-wall cell size is investigated with grid sets using fixed near-wall cells of different size ranging from the linear sub-layer to the outer edge of the log-layer. These grid sets were obtained from the grids generated for the direct application of the no-slip condition removing grid lines in the near-wall region. This means that the near-wall cells do not exhibit the smallest width. The same near-wall cell size was used in grids that exhibit a continuous increase of the cell width with the distance to the wall, which is the typical technique applied in commercial grids.

The results suggest the following conclusions:

- Wall-function boundary conditions are a very poor model for flows that exhibit a non-negligible region of laminar flow. The results obtained in such type of flows may be completely unrealistic and the iterative convergence properties may be even worse than those obtained with the direct application of the no-slip condition.
- Friction resistance coefficients obtained with wall-function boundary conditions depend on the near-wall cell size (y^+). Values of y^+ in the buffer-layer may lead to differences of 10% to the results obtained with the direct application of the no-slip condition (NS). The range of y^+ that leads to results that match the NS solution increases with the Reynolds number.
- Even at $Rn = 10^9$, we have obtained 1% difference between the skin-friction prediction with and without wall functions. This difference increases to 3% if the grids have increasing cell width with the distance to the wall. Therefore, grids for the application of wall-function boundary conditions require refinement at the edge of the near-wall cells to determine accurately the shear-stress at the wall.
- For high Reynolds numbers flows, i.e. nearly fully-turbulent flows, differences between pressure distributions obtained with and without wall functions show a much weaker dependence on the near-wall cell size than friction forces. In some cases such differences may be negligible.

Naturally, in grids with sufficiently small near-wall cells, i.e. for $y^+_{max} < 1$, automatic wall functions are (nearly) equivalent to the direct application of the no-slip condition (shear-stress at the wall obtained from its definition) and so the two approaches will lead to almost equal results. However, in such conditions wall functions are not required. Therefore, the conclusions stated above apply to situations where the near-wall cells are too large to apply NS.

The present exercise suggests that wall-function boundary conditions may be a useful mathematical model for fully-turbulent flows around complex geometries. However, it must be emphasized that when compared to the direct application of the no-slip condition the advantage is purely numerical. If friction forces are dominant, wall-function boundary conditions should be avoided.

REFERENCES

[1] Launder B. Numerical Computation Of Convective Heat-Transfer In Complex Turbulent Flows - Time To Abandon Wall Functions, *International Journal of Heat and Mass Transfer*, (1984) **27**:1485–1491.

[2] Menter, F., Esch, T. Elements of Industrial Heat Transfer Predictions, *16th Brasilian Congress of Mechanical Engineering*, (2001).

[3] Apsley D. CFD Calculation of Turbulent Flow with Arbitrary Wall Roughness, *Flow Turbulence and Combustion*, (2007) **78**:153–175.

[4] Eça L., Hoekstra M., Numerical Aspects of Including Wall Roughness Effects in the SST $k-\omega$ Eddy-Viscosity Turbulence Model, *Computer & Fluids*, (2011) **40**:299–314.

[5] Mohammadi B., Puigt G. Wall Functions in Computational Fluid Mechanics, *Computers & Fluids*, (2006) **35**:1108–1115.

[6] Craft T.J., Gerasimov A.V., Iacovides H., Launder B.E. Progress in the Generalization of Wall-Function Treatments, *International Journal of Heat and Fluid Flow*, (2002) **23**:148–160.

[7] Lacasse D., Turgeon E., Pelletier D. On the Judicious Use of the $k-\varepsilon$ Model, Wall functions and Adaptivity, *International Journal of Thermal Sciences*, (2004) **24**:925–938.

[8] Craft T.J., Gant S.E., Gerasimov A.V., Iacovides H., Launder B.E. Development and Application of Wall-Function Treatments for Turbulent Forces and Mixed Convection Flows, *Fluid Dynamics Research*, (2006) **38**:127–144.

[9] Albets-Chico X., Pérez-Segarra C.D., Oliva A., Bredberg J. Analysis of Wall-Function Approaches using Two-Equation Turbulence Models, *International Journal of Heat and Fluid Flow*, (2008) **51**:4940–4957.

[10] Wackers J., Ait Said K., Deng G.B., Queutey P., Visonneau M., Mizine I. Adaptive Grid Refinement Applied to RANS Ship Flow Computation, *28th Symposium on Naval Hydrodynamics*, (2010) California, U.S.A.

[11] Liefvendahl M., Felli M., Troeng C. Investigation of Wake Dynamics of a Submarine Propeller *28th Symposium on Naval Hydrodynamics*, (2010) California, U.S.A.

[12] Deng G.B., Visonneau, M. Comparison of Explicit Algebraic Stress Models and Second-Order Turbulence Closures for Steady Flows around Ships, *7th International Conference on Numerical Ship Hydrodynamics*, (1999) Nantes, France.

[13] Ley,J., Sigmund,S., el Moctar, O., Numerical Prediction of the Added Resistance of Ships in Waves, OMAE2014-24216 paper, *ASME 33rd International Conference on Ocean, Offshore and Arctic Engineering*, San Francisco, California, June 2014.

[14] Vaz G., Jaouen F., and Hoekstra M., Free-Surface Viscous Flow Computations. Validation of URANS Code FRESCO, *Proceedings of OMAE2009*, Honolulu, Hawaii, USA, June 2009.

[15] Menter F.R., Two-Equation Eddy-Viscosity Turbulence

Models for Engineering Applications, *AIAA Journal* 1994 **32**:1598–1605.
[16] Wilcox D.C. - *Turbulence Modeling for CFD* - DCW Industries, 2nd Edition, 1998.
[17] Eça L, Hoekstra M., On the Grid Sensitivity of the Wall Boundary Condition of the $k-\omega$ model, *Journal of Fluids Engineering*, Vol. 126,N^o 6, November 2004, pp. 900-910.
[18] Eça L, Hoekstra M., On the Application of Wall Functions in Ship Viscous Flows, *Proceedings of Computational Methods in Marine Engineering IV*, MARINE 2011, Lisbon, Portugal, September 2011.
[19] Eça L, Hoekstra M., Near-Wall Profiles of Mean Flow and Turbulence Quantities Predicted by Eddy-Viscosity Turbulence Models, *International Journal of Numerical Methods in Fluids*, (2010), **63**:953–988.
[20] http://www.refresco.org
[21] Ferziger J.H., Peric M. - *Computational Methods for Fluid Dynamics* - Springer-Verlag Berlin, 1996.
[22] Klaij C.M., Vuik C., SIMPLE-type preconditioners for Cell-Centered, Collocated Finite Volume Discretization of Incompressible Reynolds-Averaged Navier-Stokes Equations, *International Journal for Numerical Methods in Fluids*, 71(7):830–849, 2013
[23] Pereira F.S., Eça L., Vaz G., On the Order of Grid Convergence of the Hybrid Convection Scheme for RANS Codes, *Congreso de Métodos Numéricos en Ingeniería*, June 2013, Bilbao, España.
[24] Rosetti G., Vaz G., Fujarra A., URANS Calculations for Smooth Circular Cylinder Flow in a Wide Range of Reynolds Numbers: Solution Verification and Validation, *Journal of Fluids Engineering*, Vol.134, December 2012.
[25] Bandringa, H., Verstappen, R., Wubs, F., Klaij, C., van der Ploeg, A. *On novel simulation methods for complex flows in maritime applications*, 15th Numerical Towing Tank Symposium (NuTTS), Cortona, Italy, 2012.
[26] Hawkes, J., Vaz, G., Turnock, S., Cox, S., and Philips, A., Software Performance Analysis of Massively-Parallel Hydrodynamics Simulations, *In Proceedings of 11th International Conference on Hydrodynamics (ICHD)*, Singapore, October, 2014.
[27] Eça L., Hoekstra M., A Procedure for the Estimation of the Numerical uUncertainty of CFD Calculations Based on Grid Refinement Studies, *Journal of Computational Physics*, Vol. 261 April 2014, pp-104-130.
[28] Eça L., Hoekstra M. The Numerical Friction Line, *Journal of Marine Science and Technology*, Vol. 13, Number 4, 2008, pp-328-345.
[29] Schlichting H., Boundary Layer Theory, *McGraw-Hill*, (1979), Seventh Edition.
[30] http://turbmodels.larc.nasa.gov/
[31] Eça L., Vaz G., Workshop on Verification and Validation for Offshore Flows, *Proceedings of the ASME 2012 31st International Conference on Ocean, Offshore and Arctic Engineering*, OMAE2012 July 1-6, 2012, Rio de Janeiro, Brazil
[32] Eça L., Vaz G., Rosetti, G., Pereira, F., On the Numerical Prediction of the Flow Around Smooth Circular Cylinders, *ASME 33rd International Conference on Ocean, Offshore and Arctic Engineering*, San Francisco, California, June 2014.